JGR Oceans

RESEARCH ARTICLE
10.1029/2018JC014636

Temporal and Spatial Hydrodynamic Variability in the Mallorca Channel (Western Mediterranean Sea) From 8 Years of Underwater Glider Data

Bàrbara Barceló-Llull[1], Ananda Pascual[1], Simón Ruiz[1], Romain Escudier[2], Marc Torner[3], and Joaquín Tintoré[1,3]

[1]IMEDEA (UIB-CSIC), Esporles, Spain, [2]CMCC, Bologna, Italy, [3]SOCIB, Palma de Mallorca, Spain

Key Points:
- High-frequency variability dominates the circulation and transport across the channel
- The characteristic horizontal dimension of mesoscale instabilities in this region is 6.0 km
- Two-way flow controls the annual cycle of the transport of water with prevalence of the inflow of Atlantic water

Correspondence to:
B. Barceló-Llull,
b.barcelo.llull@gmail.com

Citation:
Barceló-Llull, B., Pascual, A., Ruiz, S., Escudier, R., Torner, M., & Tintoré, J. (2019). Temporal and spatial hydrodynamic variability in the Mallorca channel (western Mediterranean Sea) from 8 years of underwater glider data. *Journal of Geophysical Research: Oceans*, *124*, 2769–2786. https://doi.org/10.1029/2018JC014636

Received 4 OCT 2018
Accepted 17 FEB 2019
Accepted article online 20 FEB 2019
Published online 24 APR 2019

Abstract Eight years of glider data are used to characterize the temporal and spatial variability of a region in the western Mediterranean that will constitute one of the targets for the calibration phase of the Surface Water and Ocean Topography (SWOT) satellite mission. The characteristic horizontal dimension of mesoscale instabilities in the Mallorca channel is 6.0 km. The temporal evolution of intermediate water masses is dominated by an increase over time of the characteristic temperature values. Western Mediterranean and Levantine Intermediate waters display an increase of the temperature extrema of 0.064 ± 0.002 and 0.044 ± 0.002 °C/year between 2011 and 2018, respectively. At the layer of Levantine Intermediate water the salinity temporal regression reveals a mean trend of 0.010 year^{-1}. Temperature annual cycle shows an averaged temperature gradient of ~6 °C in 6 months at the upper layer, with a disconnection with the annual cycle at 100-m depth. The circulation across the channel is dominated by high-frequency variability. The signature of eddies with radius ranging from 5 to 18 km is apparent in 16% of the transects analyzed and mainly in spring and summer, with a dominance of subsurface cyclonic eddies. Two-way flow controls the annual cycle of the water transport through the channel with prevalence of the inflow of Atlantic water. Variations of water transport over timescales of weeks to months can be similar to those identifiable as seasonal changes.

Plain Language Summary Eight years of glider data are used to characterize the temporal and spatial variability of a region in the western Mediterranean that will constitute one of the targets for the calibration phase of the forthcoming Surface Water and Ocean Topography (SWOT) satellite mission. Our results demonstrate that in the Mallorca channel the horizontal dimensions of the scales that SWOT aims to resolve may be as small as 6 km. We observe that the water masses that reside at intermediate layers are increasing their temperature and salinity extrema over time. Temperature annual cycle shows an averaged temperature gradient of ~6 °C in 6 months at the upper layer, with a disconnection with the annual cycle at 100 m. Dynamic variability at shorter temporal scales is more intense than the annual cycle. Small coherent features are observed in spring and summer, with radius ranging from 5 to 18 km. The transport of water through the channel is characterized by the inflow of recent Atlantic water and the outflow of local Atlantic water. Understanding the hydrodynamics of this region will have an important contribution to the calibration phase of the SWOT satellite mission, the next big breakthrough in Earth observation.

1. Introduction

The Balearic Islands constitute a natural boundary between two subbasins of the western Mediterranean Sea: the Balearic subbasin in the north and the Algerian subbasin in the south (Figure 1). The center of the Balearic subbasin is mainly characterized by the presence of surface local Atlantic water (local AW) already modified by a long stay in the Mediterranean (Hopkins, 1978; Pinot et al., 2002; Balbín et al., 2012). Below the upper layers, the hydrography of the Balearic subbasin is constituted by the following water masses: Western Mediterranean Intermediate water (WIW) formed in the northwestern Mediterranean in winter and defined by a relative minimum of temperature, Levantine Intermediate water (LIW) originated at the eastern Mediterranean and characterized by maxima of salinity and temperature, and Western Mediterranean Deep water (WMDW) formed during deep winter convection events is the northwestern Mediterranean (MEDOC-Group, 1970; López-Jurado et al., 2008). The Algerian subbasin is influenced by the inflow of

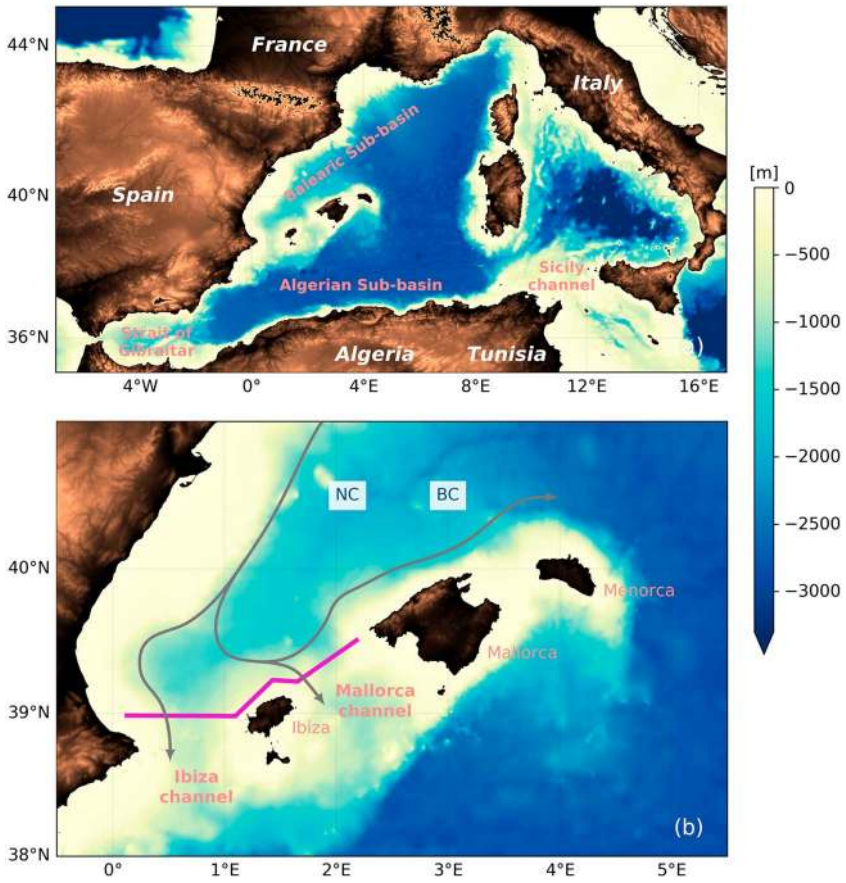

Figure 1. (a) Map of the western Mediterranean Sea with the topography of the region (SRTM30+ version 6.0, ; Becker et al., 2009). (b) Region of study with the main currents of the Balearic subbasin. Magenta line represents the glider trajectory followed during Canales missions.

fresher and warmer surface Atlantic water coming from the Strait of Gibraltar (recent AW) and is characterized by intense dynamics with energetic density fronts and gyres (Font, 1990; Pascual & Gomis, 2003; Testor et al., 2005; López-Jurado et al., 2008; Escudier, Mourre, et al., 2016; Lana et al., 2016).

The exchange of water between these two subbasins is mediated by the Mallorca and Ibiza channels (Figure 1), which play a key role in the regional circulation of the western Mediterranean (Pinot et al., 2002). The surface circulation of the western Mediterranean is mainly cyclonic at the basin scale and is driven by the Northern current (NC), flowing southwestward along the French and Spanish coasts, and by the Algerian current that flows along the Algerian shore (Ruiz et al., 2002; Testor et al., 2005; Pascual et al., 2014). In the Balearic subbasin (Figure 1b), the NC is divided into two branches, one flowing through the Ibiza channel and leaving the Balearic subbasin and the other recirculates cyclonically forming the Balearic current (Pinot et al., 2002; Pascual & Gomis, 2003; Ruiz et al., 2009). Recent AW enters the Balearic subbasin through the Mallorca and Ibiza channels from the Algerian subbasin. The warmer and fresher inflow of recent AW feeds the Balearic current, which flows northeastward along the northwestern coasts of Ibiza, Mallorca, and Menorca (Pinot et al., 1995; Ruiz et al., 2009). Eddies with different sizes are common dynamical features of the Balearic circulation. They are formed locally or advected by the NC (e.g., Pascual et al., 2002; Bouffard et al., 2012; Amores et al., 2013; Mason & Pascual, 2013; Bosse et al., 2016; Escudier, Renault, et al., 2016). The exchange of water masses through the island channels has been shown to have an impact on the development of mesoscale eddies within the Balearic subbasin (Pascual et al., 2002; Amores et al., 2013). The inflow of recent AW may be enhanced by the presence of gyres into the Algerian subbasin, while the circulation through the island channels can be interrupted by the presence of eddies within the Balearic subbasin (Pinot et al., 2002; Ruiz et al., 2002; Amores et al., 2013; Escudier, Mourre, et al., 2016). The frontal mixing of water masses near the island channels has also an impact on the abundance and distribution of

tuna and constitutes an important component of the Balearic archipelago ecosystem that has been recognized as one of the main spawning areas of the stock in the eastern Atlantic of the Atlantic bluefin tuna, with high commercial interest (Alemany et al., 2010).

The Canales project at the Balearic Islands Coastal Ocean Observing and Forecasting System (SOCIB, Tintoré et al., 2013) started in 2011 with the objective to monitor the circulation of the Mallorca and Ibiza channels. Currently, the Canales project provides glider data of the island channels with a maximum time gap between missions of 1 month. A typical Canales mission consists on the deployment of a glider close to the Mallorca coast (Figure 1b). Then the glider navigates to the Ibiza coast along the Mallorca channel. Finally, the glider samples the Ibiza channel with several sections and returns to the Mallorca island following the same path. The first years of glider data have been used to study the water transport variability in the Ibiza channel (Heslop et al., 2012; Heslop, 2015) and to validate the SOCIB operational ocean forecasting system (Juza et al., 2015, 2016). Heslop et al. (2012) analyze glider data between January and June 2011, and they demonstrate that the variations in the transport of water through the Ibiza channel over timescales of days to weeks can be as large as those previously identified as seasonal or eddy driven. More recently, Juza et al. (2019) analyzed glider data from 2011 to 2017 in the Ibiza channel to define an innovative geometry-based method to detect WIW, and to analyze the variability of this water mass. Despite the availability of this long temporal series of glider data, the Mallorca channel has not yet been studied in detail.

The forthcoming Surface Water and Ocean Topography (SWOT) satellite mission is the next big breakthrough in Earth observation and aims to provide high-resolution sea surface height measurements in two dimensions along a wide-swath altimeter (Fu & Ferrari, 2008; Fu & Ubelmann, 2013). The wide-swath SWOT altimeter will allow unique observations in the wavelength scales between 15 and 100 km, gathering in some regions small mesoscale and submesoscale dynamics. The Mediterranean Sea is a region characterized by smaller spatial scales than those observed at similar latitudes in other parts of the world ocean (Beuvier et al., 2012; Escudier, Renault, et al., 2016; Gómez-Navarro et al., 2018). Understanding fine-scale dynamics in this region is particularly challenging because of the smaller scales and also due to intense mesoscale and submesoscale dynamics that interact and modulate basin-scale circulation (Pinot et al., 2002; Ruiz et al., 2009; Pascual et al., 2017). During the fast-sampling phase after launch, SWOT will provide daily high-resolution sea surface height measurements in selected areas of the world ocean for instrumental calibration/validation purposes. These data will be compared with independent observations from both in situ and remote sensing platforms. The region around the Balearic Islands constitutes one of the targeted areas for the SWOT fast-sampling phase, becoming an interesting region of study to anticipate the SWOT launch (Barceló-Llull et al., 2018).

The goal of this study is to characterize a region in the western Mediterranean Sea that will be sampled at high spatial and temporal resolution by the SWOT satellite mission during the fast-sampling phase after launch in 2021 (Fu et al., 2009). Our aim is to analyze the temporal and spatial hydrodynamic variability of the Mallorca channel using 8 years of glider data (Schaeffer et al., 2016; Rudnick et al., 2017). This first effort to characterize the region targeted for the SWOT fast-phase focuses on physical variables, as temperature, salinity, and velocity. The paper is organized as follows. In section 2 we describe the glider data used for this study. Then, we present the results in five sections. First, we estimate the dominant length scale of mesoscale dynamics in order to evaluate the capability of SWOT to reach the submesoscale. We continue with the analysis of the interannual temporal evolution of the water masses in this important choke point of the western Mediterranean. Temporal series of temperature, salinity, and geostrophic velocity are then analyzed to estimate for each variable a mean field, a linear tendency, and an annual cycle. The mean field of geostrophic velocity reveals an intensified inflow of recent AW near the Mallorca coast, and a weaker outflow of local AW near Ibiza. The higher-frequency variability observed in vertical sections of geostrophic velocity is investigated in sections 3.4 and 3.5. First, we analyze the presumable signal of eddies with different horizontal dimensions crossing the channel. Then, we analyze the temporal variability of the transport of water highlighting an overlying of the annual cycle by higher-frequency variability. Finally, we summarize our main findings.

2. Data and Methods

Since 2011, SOCIB and IMEDEA Slocum gliders have surveyed the Mallorca and Ibiza channels in the framework of the Canales project. This long-term monitoring program has collected 55 transects of glider data across the Mallorca channel during 8 years of glider missions distributed equally by seasons and covering all months (Figure 2). Measured variables include pressure, temperature, and salinity. Raw glider data were processed with the SOCIB Glider Toolbox, which includes thermal lag correction and quality control (Troupin et al., 2015). In addition, sensors mounted aboard the gliders deployed in the Canales missions have been maintained according to the recommendations of both glider and sensors manufacturers. Since the beginning of the Canales project, gliders have been shipped back to manufacturer for factory recalibration within a maximum period of 2 years. In the Mallorca channel there is a total of 5,216 profiles (maximum depth of 958 m) with a horizontal resolution that changes with bathymetry and which is approximately 2 km in the deepest part of the 65-km-wide channel. Each transect took on average 2.8 days to be completed (Heslop, 2015).

We use the Thermodynamic Equations of Seawater (TEOS-10) functions to calculate potential temperature from in situ temperature and derived variables (Feistel, 2003, 2008). Potential temperature and practical salinity data (hereinafter temperature and salinity, respectively) have been interpolated onto a vertical resolution of 5 m and a horizontal resolution along the glider track line of 2 km. Measurement of the compass error before each glider deployment is routinely done at SOCIB only since May 2016. Because of this, the depth-averaged current measured by the glider is not corrected before this date and we assume a reference level of no motion for the geostrophic velocity inference (Bouffard et al., 2010). Dynamic height profiles have been inferred following the methodology proposed by Pinot et al. (1995) assuming a reference level of no motion at 800-m depth or the seafloor where profile depth is shallower (Heslop et al., 2012). Only transects with at least one profile deeper than the reference level have been considered for this computation; this results in 50 transects from a total of 55 with the reference level at 800-m depth. To infer the geostrophic velocity perpendicular to the transect through thermal wind balance, the dynamic height was previously smoothed with a Loess filter considering a spatial scale of 15 km. The volume of water transported by the geostrophic circulation is defined as

$$Q = \int \int_S v \mathrm{d}S, \tag{1}$$

where Q is the flow, v is the component of the geostrophic velocity perpendicular to the transect, and dS is the differential of area (dS = dx dz, where dx = 2 km and dz = 5 m).

3. Results and Discussion

3.1. First Baroclinic Rossby Radius of Deformation

The first baroclinic deformation radius is related to the dominant length scale of baroclinically unstable waves within a stratified shear flow (Chelton et al., 1998) and defines a natural scale often associated with boundary dynamics, as boundary currents and fronts, and with mesoscale eddies (Gill, 1982; Hallberg, 2013; Nurser & Bacon, 2014; Escudier, Renault, et al., 2016). Through the inference of this parameter, we may evaluate the scales that SWOT will resolve in the Mallorca channel. The first baroclinic Rossby radius of deformation, λ_1, is estimated following the WKB approximation proposed by Chelton et al. (1998), which includes the effects of earth rotation, stratification, and water depth,

$$\lambda_1 \approx \frac{1}{f\pi} \int_{-H}^{-30} N(z) \mathrm{d}z, \tag{2}$$

where f is the Coriolis parameter, H is the depth of the water column, and $N(z)$ is the Brunt-Väisälä frequency defined as $N^2 = -(g/\rho_0)\partial_z \sigma_\theta$ (where g is gravity, ρ_0 is the mean density, and σ_θ is the potential density anomaly). The vertical integration is performed from the maximum depth of the profiles to the upper limit of the available data (30-m depth).

The temporal average of λ_1 (Figure 3a) shows small dependence with the depth of the water column for profiles with maximum depths deeper than 250 m, being the mean value along the distance axis for this case 6.4 km with a deviation of ±0.5 km (vs. a deviation of ±1.4 km when considering also the shallower profiles). The reason for this low dependence with depth may be that below 250 m the stratification is small while it is maximum in the upper layers (Chelton et al., 1998). The high deviation of the temporal average

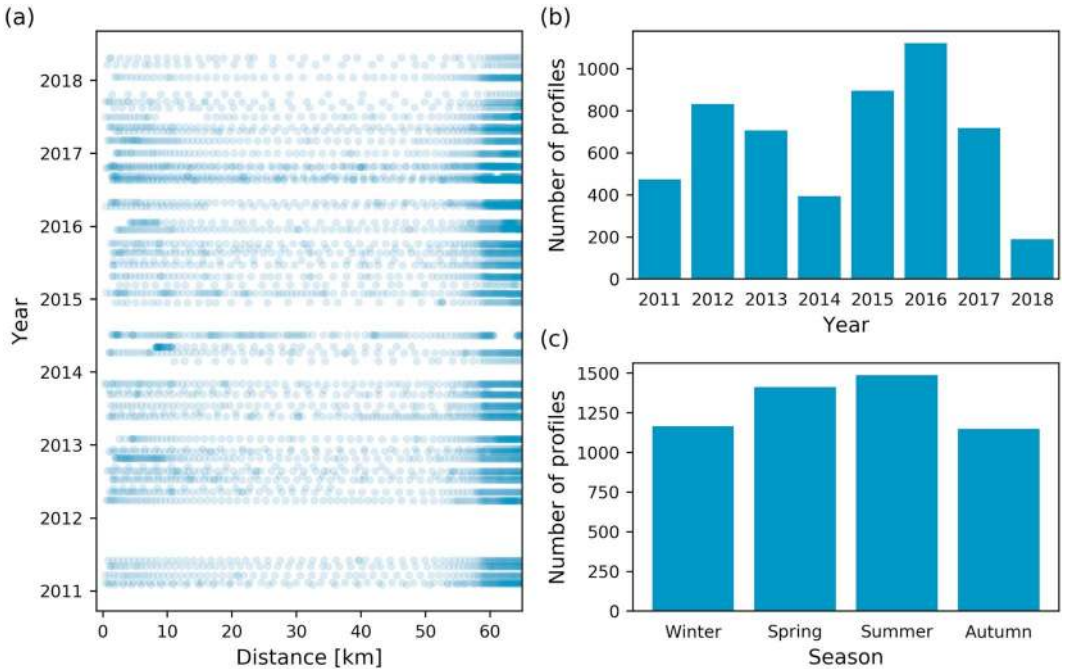

Figure 2. (a) Temporal coverage of the glider transects as a function of distance along transect from the Ibiza coast. Dots represent individual profiles from the L2 processed data. There are a total of 5,216 glider profiles collected from February 2011 to April 2018. (b) Yearly and (c) seasonal distribution of the glider profiles across the Mallorca channel.

in each point of the distance axis (blue shadow in Figure 3a) suggests an important temporal variability of λ_1 confirmed by the seasonal averages shown in Figure 3b. Considering only the profiles deeper than 250 m, during winter and spring λ_1 has values of 5.4 ± 1.0 and 5.6 ± 1.0 km, respectively, while in summer and autumn λ_1 = 7.4 ± 1.5 km and λ_1 = 7.2 ± 1.6 km, respectively. This increase of the Rossby deformation radius during summer and autumn may be due to summer heating that enhances the stratification in the upper layers. The high standard deviation of these values, especially in summer and fall, could be related to interannual variability of the stratification at the Mallorca channel and higher-frequency signal.

The western Mediterranean Sea has been previously described by relatively small Rossby deformation radius of the order of 10–15 km (Beuvier et al., 2012; Escudier, Renault, et al., 2016). At the Mallorca channel the Rossby deformation radius inferred using model simulations decreases to 9–11 km (Escudier, Renault, et al., 2016) and using climatological data representative of the end of the 1990s down to 7 km (Beuvier et al., 2012). Through glider data we estimate an average Rossby deformation radius of 6.0 ± 2.0 km, and only considering profiles deeper than 250 m λ_1 = 6.4 ± 1.6 km. These values are similar to those previously obtained within the Mallorca channel. SWOT mission aims to observe wavelength scales between 15 and 100 km, which correspond to structures with horizontal dimensions between 4 and 25 km. Gómez-Navarro et al. (2018) evaluate the SWOT capacity to resolve fine-scale structures in the western Mediterranean. After the application of a Laplacian diffusion filter to remove satellite noise on simulated SWOT data, they suggest that SWOT may be able to resolve wavelength scales down to 40–60 km. Considering this value, in the western Mediterranean SWOT may observe surface structures with horizontal dimensions higher than 10–15 km. Given that the inferred dominant horizontal dimension of mesoscale structures in the Mallorca channel is λ_1 = 6.4 ± 1.6 km (considering profiles deeper than 250 m), we may argue that in this region SWOT will be able to resolve the large mesoscale.

The fundamental hypothesis of the linear theory that defines the baroclinic Rossby deformation radius assumes that the effects of temporal variability of the stratification are small. Chelton et al. (1998) investigated this assumption through the inference of the Rossby deformation radius using a global 1° × 1° climatology whose processing included horizontal spatial smoothing of the order of 1,000 km. Through a harmonic fitting they analyzed the annual cycle and they found that the amplitude of annual variability represented typically 1–2% of the annual mean, hence giving an indication of the significance of the amplitude of seasonal variations. In that case, the vertical extension of the climatology profiles was deep enough to

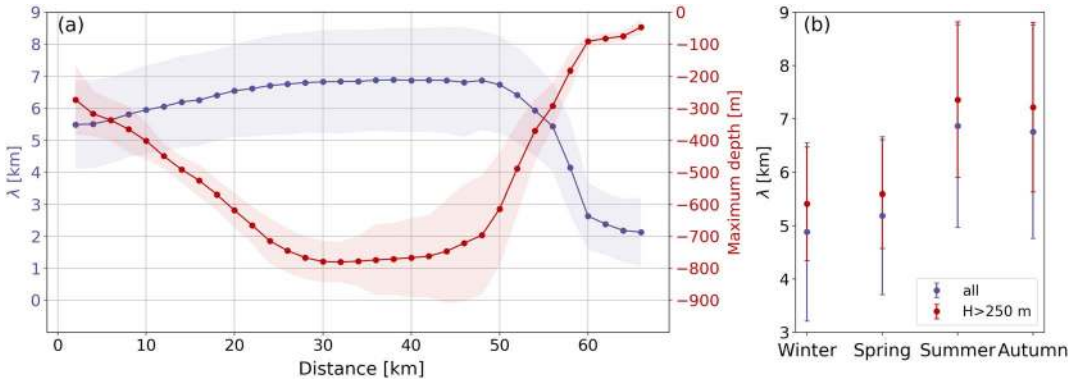

Figure 3. (a) First baroclinic Rossby radius of deformation (Chelton et al., 1998) as a function of distance from the Ibiza coast at 30-m depth averaged for all transects (blue line) and the corresponding standard deviation (blue shadow). The red line shows the averaged maximum depth of the profiles at each position along the distance axis with the corresponding standard deviation (red shadow). (b) Seasonal averages and standard deviations of the Rossby radius of deformation at 30-m depth considering all profiles (blue) and only taking into account the profiles deeper than 250 m (red).

justify that seasonal variations of the density structure were restricted only to a small fraction of the water column. Hence, the effect of the variations of $N(z)$ on the vertical over the entire water column was small. Also, they explain that in some regions as in the Gulf Stream the smoothing of the climatology avoided an accurate representation of the density field. Following the same methodology and with higher resolution, we find that seasonal variations of the Rossby deformation radius in the Mallorca channel represent 20–26% of the annual mean for profiles deeper than 250 m. These results suggest the importance of the water column depth and the resolution of the fields to determine the implications of the seasonal stratification into the inference of the Rossby deformation radius.

3.2. Temporal Evolution of the Water Masses

To analyze the interannual evolution of the water masses residing in the Mallorca channel, temperature-salinity (θ/S) diagrams per year of available glider data are represented in Figure 4. During the period 2011–2013 the residence of WIW and LIW in the Mallorca channel is demonstrated by local extrema in temperature and salinity. The WIW is characterized by a relative minimum in temperature, while the LIW is defined by a relative maximum in temperature and salinity. In 2014 there is no evidence of the tail of WIW, but the signal of LIW is apparent. From 2015 to 2018 the relative minimum of temperature defining the WIW is higher than in the previous years highlighting a warming of this water mass during the period analyzed. Also, between 2015 and 2018 the LIW maxima of temperature and salinity have higher values than in the preceding period. Considering the local characteristic values of the water masses provided by López-Jurado et al. (2008) for the period 2003–2004, during 2011–2013 the WIW temperature is maintained below 13 °C, while between 2015 and 2018 this relative minimum increases to values higher than 13 °C. Regarding the relative maxima of temperature and salinity defining the LIW, for the first period analyzed they are below the previously established upper limits of 13.4 °C and 38.60, respectively. In 2015 and 2016 the LIW temperature increases to values higher than 13.4 °C, while during the last 2 years it is near this limit. The LIW salinity maximum is maintained around 38.60 after 2015. Over the period analyzed, there is no evidence of WMDW with temperature values ranging between 12.7 and 12.9 °C, the previously defined limits of this water mass. The local AW is apparent below 100 m in all the period except in 2013 and 2014 (not shown).

The warming of intermediate waters during the period 2011–2018 is highlighted in the temporal evolution of their temperature extrema (Figure 5). The WIW minimum temperature has a tendency to increase 0.064 ± 0.002 °C/year, while the core of LIW defined by the salinity maximum between 300- and 700-m depth has increased its temperature 0.044 ± 0.002 °C/year between 2011 and 2018. These long-term trends for intermediate waters are similar to that computed in the Sicily channel through the analysis of mooring data. Schroeder et al. (2017) reported a temperature trend at 400-m depth of 0.064 °C/year between winter 2010/2011 and spring 2016. This suggests that intermediate waters are increasing their temperature at similar rates in regions of the central and western Mediterranean Sea, with trends at least an order of mag-

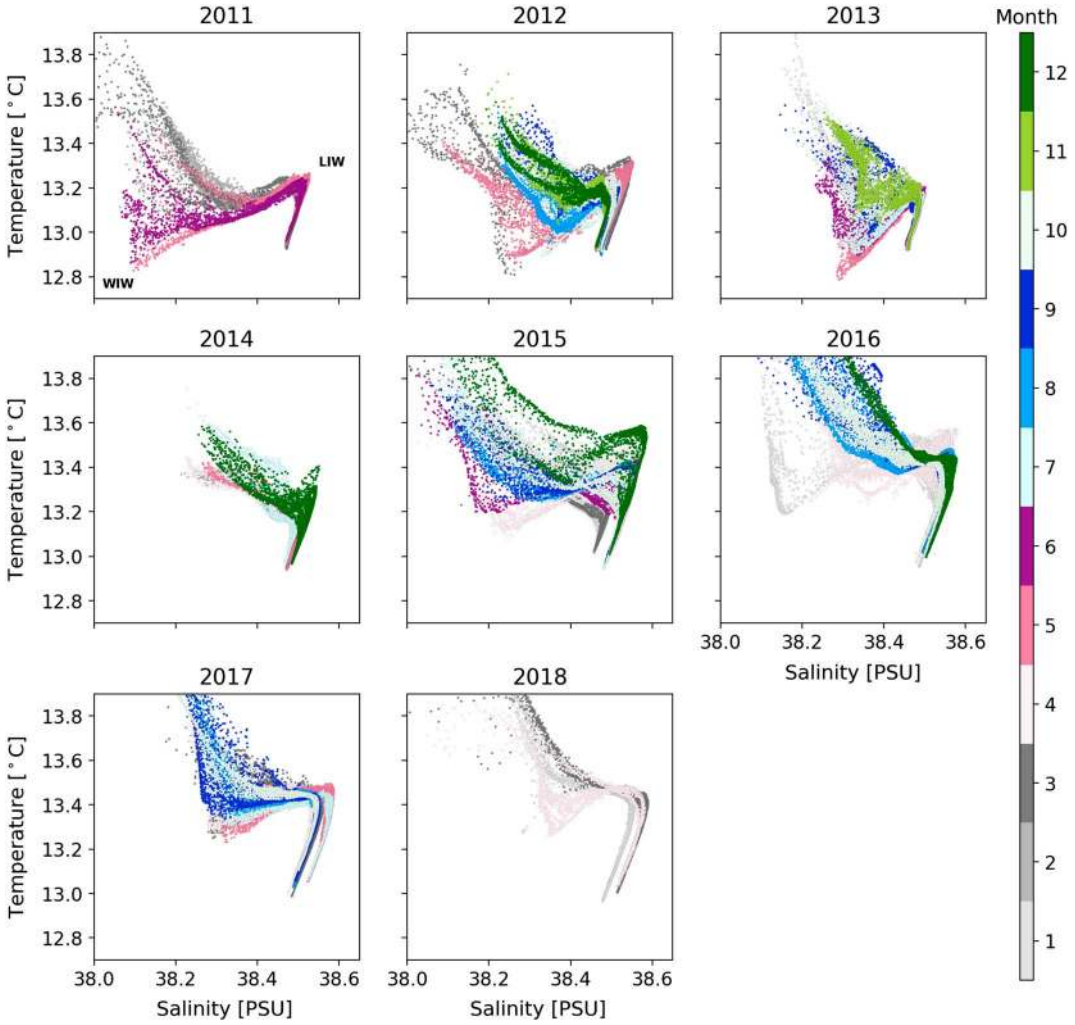

Figure 4. θ/S diagrams per year of all interpolated glider profiles centered at intermediate and deep waters. Colors represent the month of the profile.

nitude higher than the trends reported for the global ocean intermediate layer (e.g., Levitus et al., 2012). The demonstrated fast response to changing climate of the Mediterranean Sea may contribute to this increase of temperature (Schroeder et al., 2017). Also, the warming of intermediate waters in the Mallorca channel may be related to the lack of occurrence of a deep winter convection event in the northwestern Mediterranean during the last years (Marshall & Schott, 1999; Houpert et al., 2016; Testor et al., 2018). A deep winter convection event would induce the mixing and cooling of the whole water column and, hence, the cooling of the different water masses present in the region. If the increasing import of heat from the eastern to the western Mediterranean Sea through intermediate waters is maintained over time, this would have important implications in the formation of warmer deep waters in the dense water formation region of the Gulf of Lions, and in the Mediterranean Outflowing Water thermohaline characteristics (Schroeder et al., 2017).

3.3. Hydrodynamic Temporal Variability

Temporal series of temperature, salinity and geostrophic velocity are analyzed to estimate for each variable a mean field, a linear tendency, and an annual cycle. At each grid point a harmonic function with a linear term is fitted to each variable,

$$A_0 + A_t t + A_c \cos(2\pi t/T) + A_s \sin(2\pi t/T), \tag{3}$$

where A_0 is the mean field, A_t is the tendency, the period of the annual cycle is $T = 365.25$ days, the amplitude is defined as $[A_c^2 + A_s^2]^{1/2}$, and the phase as $\phi = \arctan(-A_s/A_c)$ (Rudnick et al., 2017). Averaged vertical profiles of the skill of the regression, defined as 1 − var(residuals)/var(original), obtained from fitting

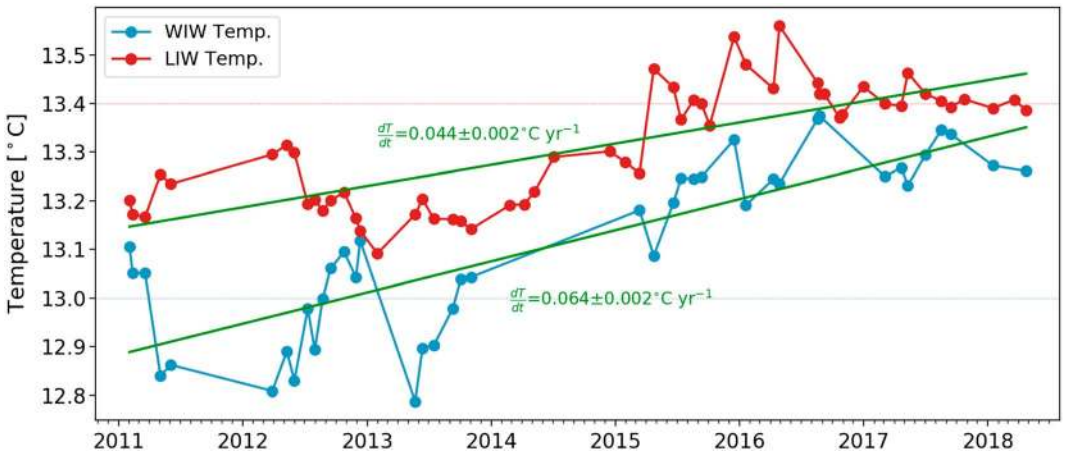

Figure 5. Temporal evolution of the minimum temperature observed between 100- and 300-m depth in transects with WIW (blue dots), and temporal evolution of the LIW core temperature defined by the maximum in salinity between 300- and 700-m depth (red dots). Thin blue (red) dotted line represents the reported higher value of the WIW (LIW) temperature for the period 2003–2004 (López-Jurado et al., 2008). Green lines represent the linear fit of the temporal evolution of each water mass temperature for the whole period analyzed. For each trend line the trend value is given with the 95% confidence interval. LIW = Levantine Intermediate water; WIW = Western Mediterranean Intermediate water.

this function to the temporal series of each variable are plotted in Figure 6 (solid lines). The skill of the temperature regression has a mean value of 0.68 and is statistically significant in the whole water column. The salinity regression is not statistically significant in the upper ~160 m; from this depth the skill increases to values higher than 0.6 below 500 m. The geostrophic velocity regression has a mean skill of 0.06 and is not statistically significant. To isolate the contribution of the linear trend, dashed lines in Figure 6 show the skill of the linear regression ($A_0 + A_t t$) for each variable. For temperature and salinity time series, the skill of the linear regression represents on average 90% of the skill of the full regression for the depth range where they are statistically significant. The lower values of the temperature linear regression skill are found in the upper layers, where it decreases to 27% of the total skill, highlighting the important contribution of the seasonal cycle in the upper layers. The skill of the geostrophic velocity linear regression is not statistically significant, suggesting the key role that high-frequency variabilities may have in this region.

Constants in the least squares fits of temperature, salinity, and geostrophic velocity represent the mean fields of these variables (Figure 7). The mean section of temperature (Figure 7a) has minimum values of 12.9 °C at the bottom of the channel and maximum values of 17.6 °C at the upper layer, while the stratification is maximum in the upper 100-m depth. The mean salinity field (Figure 7b) has minimum values of 37.9 at the upper layer on the eastern side of the Mallorca channel, while maximum values higher than 38.45 are observed below 300-m depth. This layer of homogeneous high salinity is the signal of LIW that is formed in the eastern Mediterranean and is present during the entire year in the Balearic subbasin (López-Jurado et al., 2008). The mean circulation (Figure 7c) is characterized by an intensified northwestward flow near the Mallorca coast with maximum velocities of 0.08 m/s that introduces recent AW into the Balearic subbasin. Near the Ibiza coast, a weaker southeastward flow with maxima of −0.015 m/s is indicative of an outflow of water from the Balearic subbasin to the Algerian subbasin and may be a branch of the NC.

The linear terms explain an important part of the temperature and salinity temporal variances. To analyze these tendencies, the distributions of the trend coefficients (A_t) obtained from fitting the temporal series of temperature and salinity are plotted in Figure 8. The temperature trend has maximum values in the upper ~100 m reaching up to 0.19 °C/year. Below this depth the trend decreases to a mean value of 0.077 °C/year between 100 and 300 m. At the layer of residence of LIW (300- to 700-m depth) the temperature has an average trend of 0.043 °C/year and a maximum value of 0.062 °C/year, while the mean salinity trend is 0.010 year^{-1} and maximum values reach up to 0.016 year^{-1}. The trends obtained with the regression analysis of the time series of temperature and salinity are similar to the trends computed by Schroeder et al. (2017) in the Sicily channel. They observe a salinity trend of 0.014 year^{-1} at 400-m depth between winter 2010/2011 and spring 2016, the same order of magnitude as the trends estimated at the Mallorca channel. Hence, the

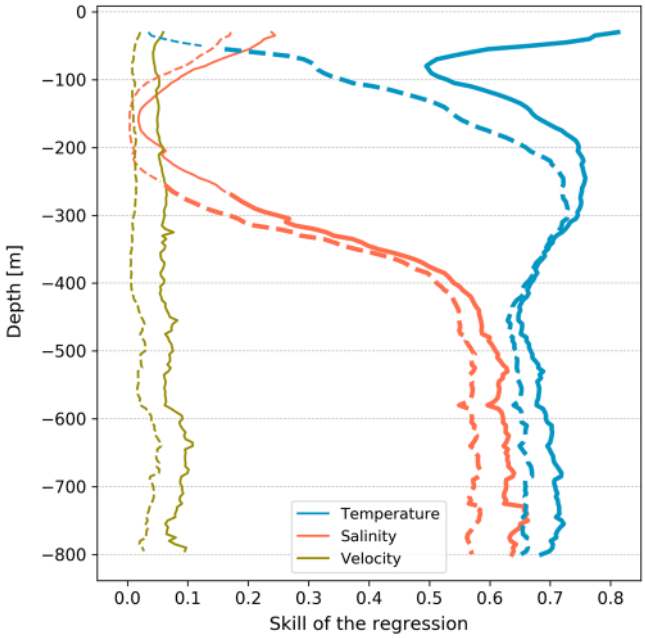

Figure 6. Averaged vertical profiles of the skill of the regression obtained from fitting the harmonic function with a linear term to the temporal series of temperature, salinity, and geostrophic velocity (solid lines), and only fitting the linear function (dashed lines). Thicker lines highlight the skill significantly different from zero (t tested with $\alpha = 0.05$).

predicted enhanced transport of salt and heat from the eastern to the western Mediterranean Sea through intermediate waters (Schroeder et al., 2017) may be corroborated by our results, with important implications in the formation of warmer and saltier deep waters in the dense water formation region of the Gulf of Lions, and in the Mediterranean Outflowing Water thermohaline characteristics (Schroeder et al., 2017).

Seasonal averages of the annual cycle including the mean fields are shown in Figure 9. Sections of temperature averaged over seasons highlight the stratification of the upper layers induced by solar heating in summer and autumn (Figures 9c and 9d), with mean temperature values at the upper layer of 20.2 and 18.8 °C, respectively. In winter the mixed layer has a mean temperature of 14.0 °C (Figure 9a), implying a seasonal variability of ∼6 °C in 6 months with respect to the summer maxima. The deeper layer is warmer in spring and cooler in autumn (note the different depths of the 13 °C isotherm). Salinity has minimum values in the upper layers ranging from 37.9 in autumn to 38.1 in spring (Figures 9d and 9b). The region saltier than 38.45 is the signal of LIW (López-Jurado et al., 2008), and its upper limit is located around 300-m depth

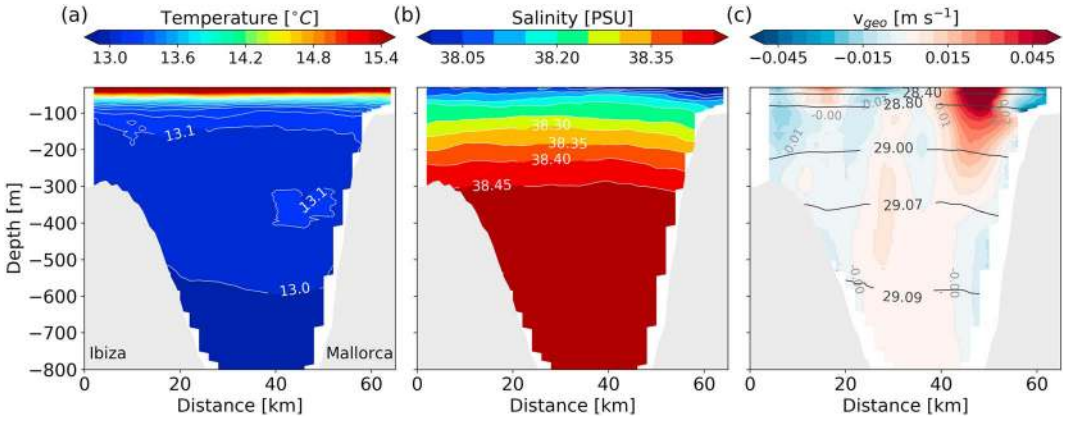

Figure 7. Vertical sections along the Mallorca channel of the mean fields of (a) temperature, (b) salinity, and (c) geostrophic velocity perpendicular to the transect. Black contours in (c) represent the mean potential density anomaly inferred from mean sections of temperature and salinity. Gray shading masks the bathymetry of the Mallorca channel. X axis represents the distance in km from the Ibiza coast.

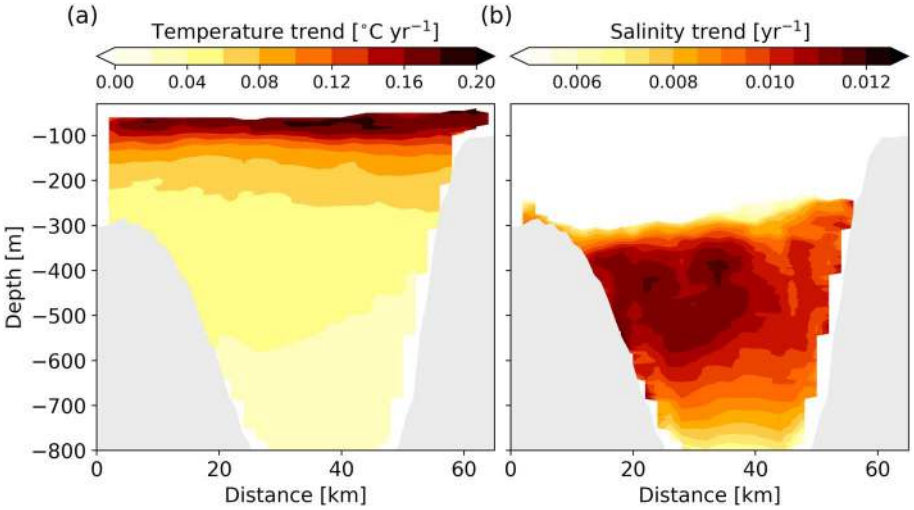

Figure 8. Vertical sections of the linear term coefficient obtained from fitting the temporal series of (a) temperature and (b) salinity. Values where the linear regression skill is not statistically significant are masked. Gray shading masks the bathymetry of the Mallorca channel. *X* axis represents the distance in km from the Ibiza coast.

in all seasons. Vertical sections of geostrophic velocity show a dominance of the northwestward flow in winter (Figure 9a), and a two-way flow in spring and summer (Figures 9b and 9c). During autumn (Figure 9d) the differentiation between the two-way flow is not as evident as in the previous seasons being the circulation pattern characterized by alternate flows with different signs. Maximum values of velocity are observed at the eastern side of the channel in all seasons, with higher speed and a more localized pattern in summer. The outflow of water from the Balearic subbasin through the Mallorca channel is generally less intense than the inflow of recent AW. In the upper 400 m recent AW introduces a signal of fresher water at the eastern side of the channel (Figure 9).

Sections at constant depth of the annual cycle anomaly allow variables to be analyzed as functions of distance from the Ibiza coast and time during the year (Figure 10). The annual cycle of temperature at 30-m depth (Figure 10a) evidences that the near-surface temperature is driven by the annual cycle of surface heat flux, maximum in late summer and minimum in late winter. The warming and cooling arrives at the same moment along the Mallorca channel, with maxima in the middle of the channel. Below the upper layers, the annual cycle of temperature shows the maximum in December, and the minimum in June, indicating a lag of 3 months with respect the upper layer annual cycle (Figure 10c). The annual cycle anomaly of salinity in the upper layer shows a lag of 1 month with respect to the temperature cycle (Figure 10b). The salinity anomaly is maximum in spring and minimum in fall along the Mallorca channel, with maxima situated at the eastern side where the variability of the inflow of recent AW may induce higher anomalies to the mean values. At 100-m depth, the maximum anomaly is detected in June near the Ibiza coast and in July near the Mallorca coast (Figure 10d). Minimum values are observed in December and January, respectively, on each side of the channel. The negative anomalies detected at 100-m depth near the Mallorca coast may be related to the deepening of the inflow of recent AW observed in autumn and winter (Figures 9d and 9a).

3.4. Eddies Within the Mallorca Channel

Vertical sections of geostrophic velocity perpendicular to the channel reveal the high-frequency variability that characterizes the region (e.g., Pinot et al., 2002). Eddies are a particular type of this variability and are characterized by a depression or uplift of the isopycnals with an anticyclonic or cyclonic circulation, respectively. The signal of localized symmetric dipolar structures of geostrophic velocity with values higher than 0.05 m/s, and the corresponding displacement of the isopycnals, are detected in 8 of the 50 transects, suggesting the presence of eddies with different sizes and intensities crossing the channel (McWilliams, 1985; Bosse et al., 2015, 2016). For instance, the cyclonic eddy detected on 9 September 2013 (Figure 11b) has a speed-based radius (half of the distance between the two velocity extrema) of 12 km, with peak geostrophic velocities of 0.14 m/s. A smaller subsurface cyclonic eddy with a radius of 7 km identified on 9 May 2012 (Figure 11a) has peak velocities of 0.21 m/s at 70-m depth. In this particular case, the eddy is not completely represented by the geostrophic velocity field, and the characteristic values summarized in Table 1 are

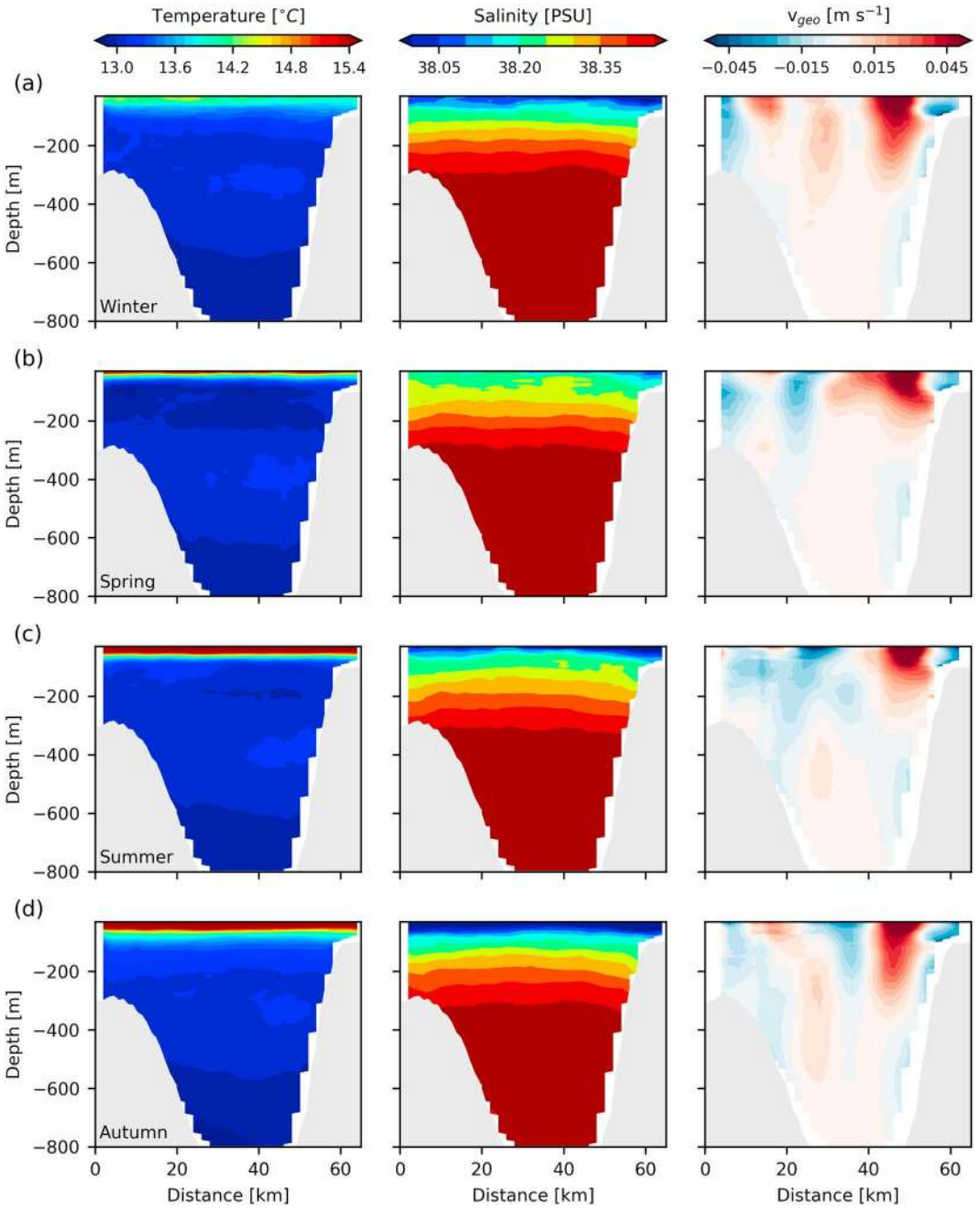

Figure 9. Seasonal averages of temperature, salinity, and geostrophic velocity perpendicular to the transect. Seasons are defined as follows: (a) January/February/March is winter, (b) April/May/June is spring, (c) July/August/September is summer, and (d) October/November/December is autumn. Gray shading masks the bathymetry of the Mallorca channel. *X* axis represents the distance in km from the Ibiza coast.

inferred with the available data. In this sense, it is important to note that the eddy may extend to the Ibiza coast having higher radius and minimum velocities. All the other eddies included in Table 1 are well represented by the geostrophic velocity and density fields, disregarding all the cases in which the eddy signature is not completely represented by the geostrophic velocity or not showing a clear symmetric pattern.

The subsurface maximum of geostrophic velocity is a common feature of the eddies crossing the channel, but the depth of maximum speed is different in each eddy (Table 1). For instance, the eddy detected on 23 August 2016 with a radius of 5 km (Figure 11c) has an intensification of the flow at ~173-m depth. A striking feature is the dominance of detected cyclonic eddies over anticyclonic eddies. Only one glider transect

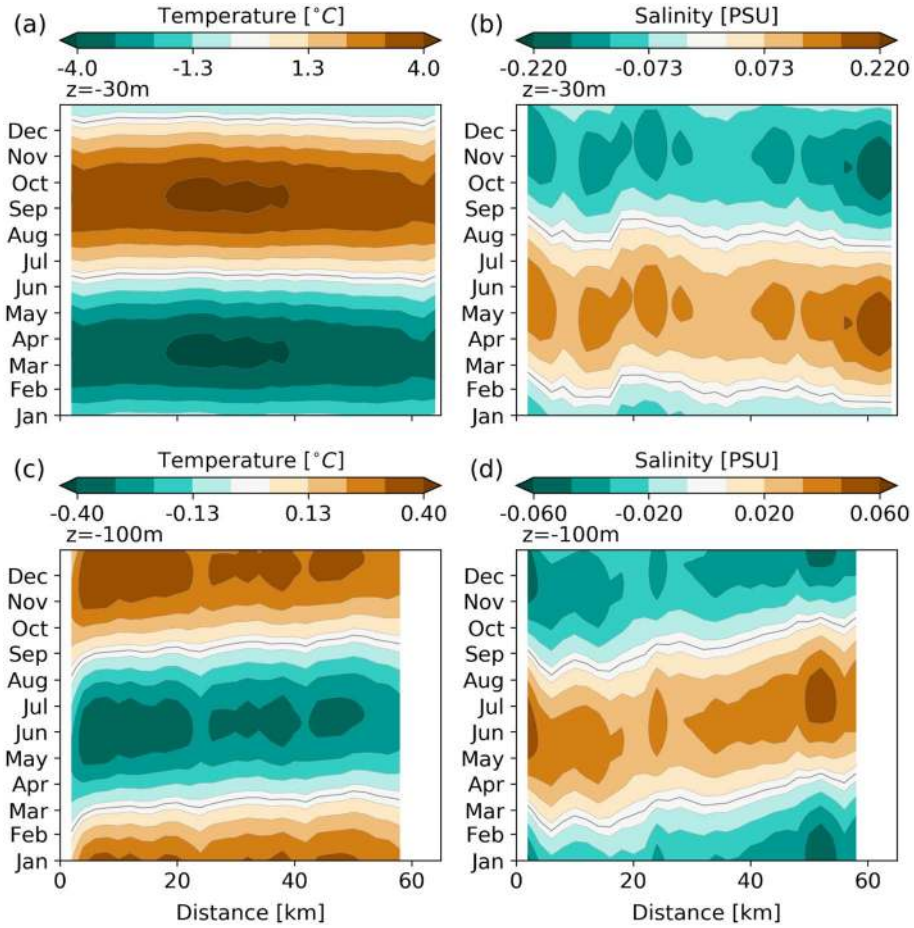

Figure 10. Annual cycle anomaly at 30-m (a, b) and 100-m (c, d) depth of temperature and salinity, respectively. The black contour represents the zero anomaly. *X* axis represents the distance in kilometers from the Ibiza coast.

evidences an anticyclonic eddy, with a radius of 18 km and maximum speed of 0.09 m/s. The magnitude of the maximum azimuthal velocity of the detected eddies ranges from 0.06 to 0.21 m/s and the radius from 5 to 18 km. The thickness of the eddies is confined between 200 and 500 m, with the maximum depth far away from the reference level assumed for the inference of geostrophic velocity. The Rossby number of these eddies has values between 0.11 and 0.65, with the higher values indicating that some eddies are moderately ageostrophic (Barceló-Llull et al., 2017). The rotation period varies from ~2.5 days for the eddies with small radius and high speed, to 14.9 days for the biggest eddy with low velocity. It should be noted that these values could be underestimated as the glider transect may not cross the eddy center (Bosse et al., 2015). Also, we should consider that gliders complete a channel sampling in 2.8 days, and the observation of these eddies is not synoptic.

Eddies are detected mainly in spring and summer with no observations in 2014 and 2015, even if in 2015 there is a high number of glider profiles (Figure 2). Similarly, in 2016, the year with more glider profiles, there is only one eddy identified. The presence of eddies crossing the Ibiza channel in spring has been reported by Heslop et al. (2012) through the analysis of glider data from January to June 2011. We may extend this finding to the Mallorca channel and suggest that the circulation at the upper and intermediate layers may be affected by the presence of eddies in spring and summer.

In the northwestern Mediterranean Sea, Bosse et al. (2015) analyzed glider data together with shipborne conductivity-temperature-depth (CTD) casts and Argo profiles from 2007 to 2013. They found anticyclonic eddies with small radius of ~5 and ~6 km in the Ligurian Sea and the Gulf of Lions, respectively. These anticyclonic eddies were characterized by homogeneous cores of LIW and lifetimes of the order of a year. Bosse et al. (2016) extended this analysis with the characterization of 18 anticyclonic eddies with different water

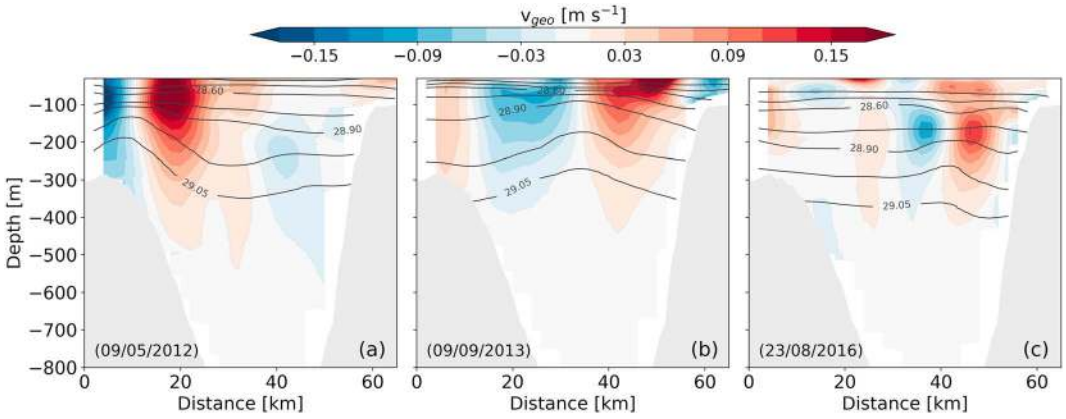

Figure 11. Vertical sections of geostrophic velocity perpendicular to the channel to illustrate some examples of eddies with different sizes and intensities observed on different dates: (a) 9 May 2012, (b) 9 September 2013, and (c) 23 August 2016. Contours represent the isopycnals: 28.0, 28.4, 28.6, 28.8, 28.9, 29.0, and 29.05 kg/m^3. Gray shading masks the bathymetry of the Mallorca channel. X axis represents the distance in km from the Ibiza coast.

masses within their cores: WIW, winter deep waters and WMDW. The peak velocities of these eddies were located at the depth range where the water masses reside. They also found the signal of 25 cyclonic eddies associated with deep convection events in the Gulf of Lions: 14 of them with subsurface intensified velocities (D_{max} ~600 m) and small radius of ~6 km, and the rest of them near-surface intensified (D_{max} ~0–100 m) with higher radius of ~8 km. The small eddies detected in the Mallorca channel together with the previous observations in the Ligurian Sea and the Gulf of Lions suggest that the presence of these coherent features with typical radius smaller than or similar to the Rossby radius of deformation is common in the western Mediterranean. In particular, in the Mallorca channel the detected eddies have radius similar to or higher than the inferred Rossby radius of deformation and may be considered mesoscale eddies. Besides the importance of these structures in the trapping and advection of water from their formation regions, only the biggest and near-surface intensified eddies may be observed by SWOT (Gómez-Navarro et al., 2018), losing a significant part of the eddies present in the region.

Although glider data allow the sampling of small eddies with high temporal and spatial coverages, eddies with higher dimensions have been also studied during the past years in the Balearic subbasin using other observational platforms. For instance, Pinot and Ganachaud (1999) using data from CTD casts along several cross-basin transects reported the presence in 1993 of an anticyclonic eddy ~50 km wide at the Mallorca channel carrying WIW within its core. In 2008 an anticyclonic eddy with a radius of ~15 km was observed

Table 1
Main Characteristics of the Eddies Identified at the Mallorca Channel

Date obs.	Type	R (km)	V_{max} (m/s)	D_{max} (m)	H (m)	Ro	T (days)
10/02/2011	C	7.0	0.20	30	350	0.62	2.5
03/05/2011	C	5.0	0.06	85	200	0.27	5.8
09/05/2012*	C	7.0	0.21	70	480	0.65	2.4
12/06/2013	A	18.0	0.09	72.5	400	0.11	14.9
09/09/2013	C	12.0	0.14	65	400	0.25	6.3
23/08/2016	C	5.0	0.12	172.5	340	0.50	3.1
16/08/2017	C	6.0	0.12	92.5	300	0.42	3.8
13/09/2017	C	7.0	0.10	120	500	0.32	4.9

Note. R is the eddy radius defined as half of the distance between the two azimuthal velocity extrema along the glider trajectory (Bosse et al., 2015). V_{max} is the mean maximum azimuthal velocity of the eddy along the glider trajectory. D_{max} is the mean depth of the azimuthal peak velocities, and H is the eddy vertical extension estimated as the region with velocities higher than 0.01 m/s. Ro = $2V_{max}/fR$ is the Rossby number and $T = 2\pi R/V_{max}$ is the rotation period. C and A indicate if the eddy is cyclonic or anticyclonic, respectively. The 09/05/2012* observation refers to the eddy shown in Figure 11a that is not completely represented by the geostrophic field and the values are inferred with the available data. Dates are formatted as DD/MM/YYYY.

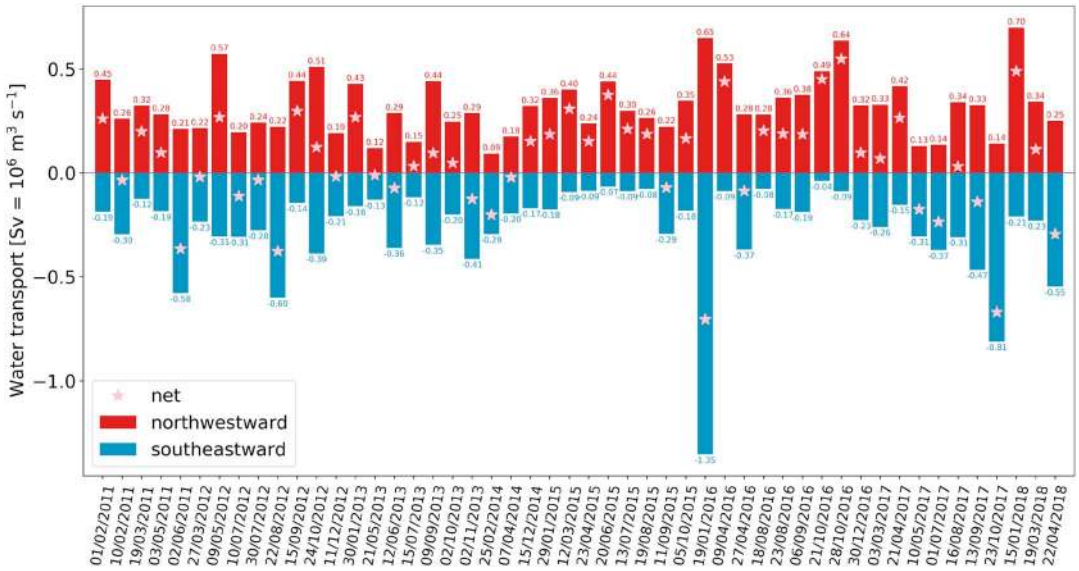

Figure 12. Geostrophic transport of water flowing northwestward (in red) and southeastward (in blue) through the Mallorca channel per glider transect. Pink stars represent the net transport. Note that glider transects are not equally distributed over time. Dates are formatted as DD/MM/YYYY.

with the combined use of modeling, altimetry, and glider data northeast of the Mallorca coast with currents of ~0.15 m/s (Bouffard et al., 2012), similar values than the biggest eddies observed at the Mallorca channel (Table 1). In the Algerian basin an anticyclonic eddy with a radius of ~20 km was sampled in 1996 by Allen et al. (2008). The presence of WIW within its core suggested the possibility that the eddy may have crossed the Ibiza channel to reach the Alboran Sea. Our study reinforces the theory that the eddies within the Balearic subbasin may enter into the Algerian subbasin through the island channels.

3.5. Transport of Water Through the Mallorca Channel

The combined effect of the different dynamical scales is manifested in the temporal evolution of the amount of water that flows through the channel. The water transport calculated for each transect is shown in Figure 12 and highlights the high-frequency variability superimposed on the annual cycle (Table 2). Seasonal averages evidence a maximum of the northwestward (NW) transport of 0.38 Sv in winter. The southeastward (SE) flow is also maximum in winter but with lower intensity than the NW flow, a ratio that is maintained in all seasons. The average of all transects displays maxima of 0.33 and −0.27 Sv for the NW (positive, inflow) and SE (negative, outflow) transports, respectively. The SE transport has similar values as the previously reported in the Ibiza channel during spring of 1989 by Castellón et al. (1990) through ADCP measurements. The flow leaving the Balearic subbasin was affected by the presence of an anticyclonic gyre and the southward flow was of −0.24 Sv. Other studies of the water transported through the Ibiza channel found higher values of the northward and southward flows, with important seasonal variability. For instance, López-Jurado and Díaz del Río (1994) found maxima of 1.08 and −0.65 Sv in November 1990 and of 0.51 and −0.56 Sv in March 1991. A more recent study carried out in the Ibiza channel (Heslop et al., 2012) found mean winter values of 0.4 and −1.0 Sv, similar to that reported by Pinot et al. (2002).

Table 2
Geostrophic Transport of Water Through the Mallorca Channel (Sv)

	Winter		Spring		Summer		Autumn		Mean	
	NW	SE	NW	SE	NW	SE	NW	SE	NW	SE
Glider analysis	0.38	−0.30	0.30	−0.26	0.29	−0.26	0.35	−0.27	0.33	−0.27
Pinot et al. (2002)	0.35	−0.30	0.32	−0.14	0.33	−0.18	0.5	−0.15	0.34	−0.18

Note. Seasonal averages and total mean. Seasons are defined as in Figure 9. NW (SE) refers to northwestward (southeastward) flow. Seasonal averages from Pinot et al. (2002) are taken from three experiments in winter, seven in spring, two in summer, and one in fall from 1996 to 1998.

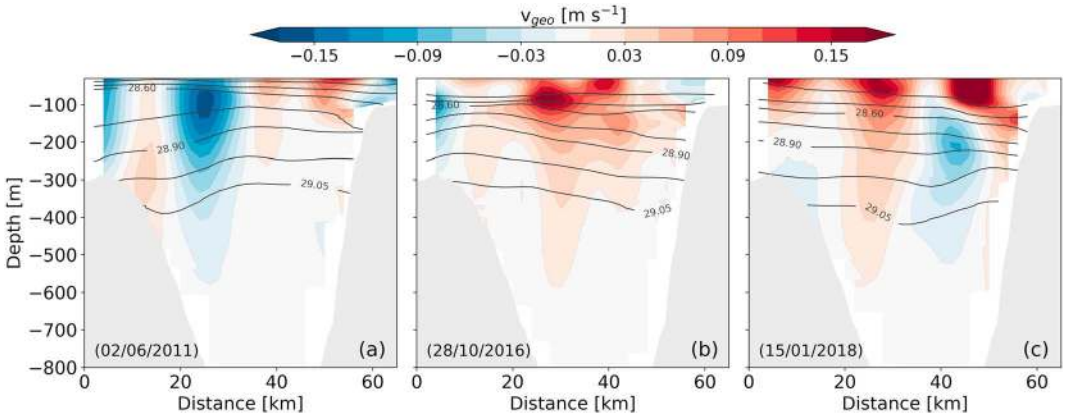

Figure 13. Vertical sections of the geostrophic velocity component perpendicular to the channel to illustrate some examples of NW and SE flows. Contours represent the isopycnals: 28.0, 28.4, 28.6, 28.8, 28.9, 29.0, and 29.05 kg/m^3. Gray shading masks the bathymetry of the Mallorca channel. *X* axis represents the distance in kilometers from the Ibiza coast.

The transport of water through the Mallorca channel is on average lower than the flow crossing the Ibiza channel, with a less pronounced seasonal variability and with smaller differences between the NW inflow and SE outflow. Although studies of the Mallorca channel are reduced in comparison with the more sampled Ibiza channel, Pinot et al. (2002) realized a 3-year-long hydrographic experiment to analyze the thermohaline circulation of both Balearic channels. Through the application of an inverse model to data collected between 1996 and 1998, they obtained similar values of water transport across the Mallorca channel than those reported here (Table 2). They identify the Mallorca channel as the preferential path of the southern waters to enter into the Balearic subbasin; this entrance of recent AW being enhanced by the occasional presence of Algerian gyres in the Algerian subbasin. Through the analysis of glider data, we also find a dominance of the NW inflow in comparison with the SE outflow; however, the mean values of the outflow are higher than those reported by them.

Long temporal series of glider data allow the examination of variations of water transport over timescales of weeks to months (Figure 12). For instance, with a difference of 10 days, the NW flow is reduced from 0.45 Sv on 1 February 2011 to 0.26 Sv on 10 February 2011, changing the sign of the net transport. Another example with a time margin of 1 month shows an abrupt decrease of the SE outflow of the order of 4 from 22 August to 15 September 2012 and an increase of the NW inflow of the order of 2. Hence, variations over timescales of weeks to months can be similar to those identifiable as seasonal changes (Heslop et al., 2012).

The complex pattern of flows illustrated in Figure 12 is influenced by the presence of (i) currents coming from the north (that are branches of the NC), (ii) eddies crossing the Mallorca channel (section 3.4), and (iii) inflow of waters from the Algerian subbasin. Although these features can be present at the same time and with different combinations within the Mallorca channel, in some cases we can differentiate the three modes or patterns (Heslop et al., 2012). Following the same nomenclature proposed for the Ibiza channel, Figure 13a shows an example of NC dominant mode, characterized by a strong southeastward current with geostrophic velocities higher than −0.15 m/s centered at 100 m and reaching down to 600-m depth. The inflow dominant mode can be observed in Figures 13b and 13c with northwestward transports of water from the surface down to 600-m depth with an intensification in the first 200 m. A combination of inflow dominant mode with outflow of water from the Balearic subbasin to the Algerian subbasin is depicted in Figure 13c. The recirculatory mode is apparent in the cases where eddies dominate the circulation within the Mallorca channel (Figure 11).

4. Conclusions

A total of 55 transects of glider data collected during 8 years of glider missions have been analyzed to characterize the temporal and spatial variability of the Mallorca channel in the western Mediterranean Sea; one of the regions targeted for the calibration phase of the SWOT satellite mission that will be launched in 2021. Glider data are used to study the characteristic horizontal dimension of mesoscale instabilities, the interannual evolution of water masses, the hydrodynamic temporal variability, the characteristics of

detected eddies, and the transport of water. The region is characterized by an averaged first baroclinic Rossby radius of deformation of 6.0 ± 2.0 km, with important seasonal variability related to summer stratification. Considering that in the western Mediterranean SWOT may resolve wavelength scales down to 40–60 km (Gómez-Navarro et al., 2018), we may conclude that in this region SWOT will reach the large mesoscale. The high standard deviations of the seasonal mean values suggest that interannual and/or high-frequency variabilities may contribute to the stratification of the water column.

Between 2011 and 2018 intermediate water masses have increased their temperature extrema. The minimum temperature of WIW shows a tendency to increase 0.064 ± 0.002 °C/year, while the maximum temperature of the LIW core has a trend of 0.044 ± 0.002 °C/year. Similar temperature trends are found in the Sicily channel at 400-m depth between 2010 and 2016 (Schroeder et al., 2017), suggesting that intermediate waters are increasing their temperature extrema at similar rates in regions of the central and western Mediterranean. These values are at least one order of magnitude higher than the global ocean intermediate water trends and may be the signal of a fast response to changing climate of the Mediterranean Sea (Levitus et al., 2012; Schroeder et al., 2017). Through regression analysis of the time series of salinity, we estimate a mean salinity trend of 0.010 $year^{-1}$ for the LIW layer, while in the Sicily channel Schroeder et al. (2017) computed a salinity trend of 0.014 $year^{-1}$ at 400-m depth. These results may corroborate the suggested increasing import of salt and heat from the eastern to the western Mediterranean Sea through intermediate waters; with important implications in the formation of warmer and saltier deep waters in the dense water formation region of the Gulf of Lions, and in the Mediterranean Outflowing Water thermohaline characteristics (Schroeder et al., 2017).

Mean circulation through the channel is dominated by an inflow of Atlantic waters located near the Mallorca coast, with maximum values of 0.08 m/s. The intensity and location of the outflow of water from the Balearic subbasin to the Algerian subbasin change throughout the year. The inflow of Atlantic waters introduces fresher and warmer water in the upper 400 m at the eastern side of the channel. Temperature annual cycle shows an averaged temperature gradient of ~6 °C in 6 months, with a disconnection between the seasonal cycle in the upper layer and at 100-m depth. In the upper layer, the temperature cycle is driven by the annual cycle of surface heat flux, while at 100-m depth the temperature maximum is observed in December and the minimum in June. Salinity has minimum values at the upper layer and are maximum in spring and minimum in autumn. The low skill of the annual regression of geostrophic velocity suggests the key role that higher frequency variabilities may have in this region. Eddies are a particular type of this variability and we have detected the plausible signal of eddies with radius ranging from 5 to 18 km in 8 of the 50 transects analyzed. These eddies are subsurface intensified (with one exception), and there is a dominance of cyclonic eddies over anticyclones. The interannual and seasonal variability of these eddies, the dominance of cyclonic over anticyclonic eddies, and the study of their formation and evolution may be the scope of future work in which it will be necessary to complement glider data with other in situ and remote sensing observations.

The combined effect of the different dynamical scales is manifested in the temporal evolution of the transport of water through the channel. The exchange of water is dominated by the inflow of Atlantic water, while the mean values of the outflow of water from the Balearic subbasin to the Algerian subbasin are higher than the values previously reported by Pinot et al. (2002). The water flowing through the Mallorca channel has on average lower intensity than the flow crossing the Ibiza channel, with a less pronounced seasonal variability and with smaller differences between the inflow and outflow. We can differentiate three modes of transport: (i) NC dominant mode, characterized by a strong southeastward transport; (ii) inflow dominant mode, identifiable as a northwestward transport of water; and (iii) recirculatory mode, in the cases where eddies dominate the circulation of the channel. The high-frequency variability of the transport of water masks the seasonal cycle; variations of water transport over timescales of weeks to months can be similar to those identifiable as seasonal changes (Heslop et al., 2012). The next challenge will be to reach temporal scales from hours to weeks and to reconstruct a three-dimensional view of the local dynamics through the development of new technologies and integrated approaches including satellite data (SWOT and SKIM (Sea surface KInematics Multiscale monitoring; Ardhuin et al., 2018)), in situ observations, and numerical modeling (Pascual et al., 2017). Future studies should consider the continuous improvement of glider data processing and quality control required to achieve the highest standards of quality.

Acknowledgments
This study is a contribution to the PRE-SWOT project (CTM2016-78607-P) funded by the Spanish National Research Program and the European Regional Development Fund (MINECO-FEDER). Glider data are freely available at the SOCIB website (https://doi.org/10.25704/jd07-sv9). We express our gratitude to the staff from SOCIB and IMEDEA who support and maintain the Canales missions. We thank Dr. Daniel L. Rudnick for fruitful discussions.

References

Alemany, F., Quintanilla, L., Velez-Belchí, P., García, A., Cortés, D., Rodríguez, J. M., et al. (2010). Characterization of the spawning habitat of Atlantic bluefin tuna and related species in the Balearic Sea (western Mediterranean). *Progress in Oceanography*, *86*(1-2), 21–38. https://doi.org/10.1016/j.pocean.2010.04.014

Allen, J. T., Painter, S. C., & Rixen, M. (2008). Eddy transport of Western Mediterranean Intermediate Water to the Alboran Sea. *Journal of Geophysical Research*, *113*, C04024. https://doi.org/10.1029/2007JC004649

Amores, A., Monserrat, S., & Marcos, M. (2013). Vertical structure and temporal evolution of an anticyclonic eddy in the Balearic Sea (western Mediterranean). *Journal of Geophysical Research: Oceans*, *118*, 2097–2106. https://doi.org/10.1002/jgrc.20150

Ardhuin, F., Aksenov, Y., Benetazzo, A., Bertino, L., Brandt, P., Caubet, E., et al. (2018). Measuring currents, ice drift, and waves from space: The Sea surface KInematics Multiscale monitoring (SKIM) concept. *Ocean Science*, *14*(3), 337–354. https://doi.org/10.5194/os-14-337-2018

Balbín, R., Flexas, M. M., López-Jurado, J. L., Peña, M., & Alemany, F. (2012). Vertical velocities and biological consequences at a front detected at the Balearic Sea. *Continental Shelf Research*, *47*, 28–41. https://doi.org/10.1016/j.csr.2012.06.008

Barceló-Llull, B., Pallàs-Sanz, E., Sangrà, P., Martínez-Marrero, A., Estrada-Allis, S. N., & Arístegui, J. (2017). Ageostrophic secondary circulation in a subtropical intrathermocline eddy. *Journal of Physical Oceanography*, *47*(5), 1107–1123. https://doi.org/10.1175/JPO-D-16-0235.1

Barceló-Llull, B., Pascual, A., Alou-Font, E., Cutolo, E., Mourre, B., Allen, J. T., et al. (2018). PRE-SWOT cruise report. Mesoscale and sub-mesoscale vertical exchanges from multi-platform experiments and supporting modeling simulations: anticipating SWOT launch (CTM2016-78607-P) (*Tech. rep.*): CSIC-UIB - Instituto Mediterrneo de Estudios Avanzados (IMEDEA). Madrid, Spain. https://doi.org/10.20350/digitalCSIC/8584

Becker, J. J., Sandwell, D. T., Smith, W. H. F., Braud, J., Binder, B., Depner, J., et al. (2009). Global bathymetry and elevation data at 30 arc seconds resolution: SRTM30 PLUS. *Marine Geodesy*, *32*(4), 355–371. https://doi.org/10.1080/01490410903297766

Beuvier, J., Béranger, K., Lebeaupin Brossier, C., Somot, S., Sevault, F., Drillet, Y., et al. (2012). Spreading of the Western Mediterranean Deep Water after winter 2005: Time scales and deep cyclone transport. *Journal of Geophysical Research*, *117*, C07022. https://doi.org/10.1029/2011JC007679

Bosse, A., Testor, P., Houpert, L., Damien, P., Prieur, L., Hayes, D., et al. (2016). Scales and dynamics of Submesoscale Coherent Vortices formed by deep convection in the northwestern Mediterranean Sea. *Journal of Geophysical Research: Oceans*, *121*, 7716–7742. https://doi.org/10.1002/2016JC012144

Bosse, A., Testor, P., Mortier, L., Prieur, L., Taillandier, V., d'Ortenzio, F., & Coppola, L. (2015). Spreading of Levantine Intermediate Waters by submesoscale coherent vortices in the northwestern Mediterranean Sea as observed with gliders. *Journal of Geophysical Research: Oceans*, *120*, 1599–1622. https://doi.org/10.1002/2014JC010263

Bouffard, J., Pascual, A., Ruiz, S., Faugère, Y., & Tintoré, J. (2010). Coastal and mesoscale dynamics characterization using altimetry and gliders: A case study in the Balearic Sea. *Journal of Geophysical Research*, *115*, C10029. https://doi.org/10.1029/2009JC006087

Bouffard, J., Renault, L., Ruiz, S., Pascual, A., Dufau, C., & Tintoré, J. (2012). Sub-surface small-scale eddy dynamics from multi-sensor observations and modeling. *Progress in Oceanography*, *106*, 62–79. https://doi.org/10.1016/j.pocean

Castellón, A., Font, J., & García, E. (1990). The Liguro-Provençal-Catalan current (NW Mediterranean) observed by Doppler profiling in the Balearic Sea. *Scientia Marina*, *54*(3), 269–276.

Chelton, D. B., deSzoeke, R. A., Schlax, M. A., El Naggar, K., & Siwertz, N. (1998). Geographical variability of the first-baroclinic Rossby radius of deformation. *Journal of Physical Oceanography*, *28*(3), 433–460. https://doi.org/10.1175/1520-0485(1998)028<0433:GVOTFB>2.0.CO;2

Escudier, R., Mourre, B., Juza, M., & Tintoré, J. (2016). Subsurface circulation and mesoscale variability in the Algerian subbasin from altimeter-derived eddy trajectories. *Journal of Geophysical Research: Oceans*, *121*, 6310–6322. https://doi.org/10.1002/2016JC011760

Escudier, R., Renault, L., Pascual, A., Brasseur, P., Chelton, D., & Beuvier, J. (2016). Eddy properties in the Western Mediterranean Sea from satellite altimetry and a numerical simulation. *Journal of Geophysical Research: Oceans*, *121*, 3990–4006. https://doi.org/10.1002/2015JC011371

Feistel, R. (2003). A new extended Gibbs thermodynamic potential of seawater. *Progress in Oceanography*, *58*(1), 43–114. https://doi.org/10.1016/S0079-6611(03)00088-0

Feistel, R. (2008). A Gibbs function for seawater thermodynamics for −6 to 80°C and salinity up to 120g kg^{-1}. *Deep-Sea Research Part I: Oceanographic Research Papers*, *55*(12), 1639–1671. https://doi.org/10.1016/j.dsr.2008.07.004

Font, J. (1990). A comparison of seasonal winds with currents on the continental slope of the Catalan Sea (Northwestern Mediterranean). *Journal of Geophysical Research*, *95*(C2), 1537–1545. https://doi.org/10.1029/JC095iC02p01537

Fu, L.-L., Alsdorf, D., Rodriguez, E., Morrow, R., Mognard, N., Lambin, J., et al. (2009). The SWOT (surface water and ocean topography) mission: Spaceborne radar interferometry for oceanographic and hydrological applications. Paper presented at OCEANOBS09 Conference, Venice.

Fu, L.-L., & Ferrari, R. (2008). Observing oceanic submesoscale processes from space. *Eos, Transactions American Geophysical Union*, *89*(48), 488–488. https://doi.org/10.1029/2008EO480003

Fu, L.-L., & Ubelmann, C. (2013). On the transition from profile altimeter to swath altimeter for observing global ocean surface topography. *Journal of Atmospheric and Oceanic Technology*, *31*(2), 560–568. https://doi.org/10.1175/JTECH-D-13-00109.1

Gill, A. E. (1982). *Atmosphere-ocean dynamics* (pp. 662). New York: Academic Press.

Gómez-Navarro, L., Fablet, R., Mason, E., Pascual, A., Mourre, B., Cosme, E., & Le Sommer, J. (2018). SWOT spatial scales in the western Mediterranean Sea derived from pseudo-observations and an ad hoc filtering. *Remote Sensing*, *10*(4), 599. https://doi.org/10.3390/rs10040599

Hallberg, R. (2013). Using a resolution function to regulate parameterizations of oceanic mesoscale eddy effects. *Ocean Modelling*, *72*, 92–103. https://doi.org/10.1016/j.ocemod.2013.08.007

Heslop, E. (2015). Unravelling high frequency and sub-seasonal variability at key ocean circulation choke points: a case study from glider monitoring in the Western Mediterranean Sea (Ph.D. Thesis), University of Southampton.

Heslop, E., Ruiz, S., Allen, J. T., López-Jurado, J. L., Renault, L., & Tintoré, J. (2012). Autonomous underwater gliders monitoring variability at "choke points" in our ocean system: a case study in the Western Mediterranean Sea. *Geophysical Research Letters*, *39*, L20604. https://doi.org/10.1029/2012GL053717

Hopkins, T. (1978). Estuarine transport processes, *chap. Physical processes of the western Mediterranean Sea* (pp. 269–309). Clemson, SC: University of South Carolina Press.

Houpert, L., Durrieu de Madron, X., Testor, P., Bosse, A., DÕOrtenzio, F., Bouin, M. N., et al. (2016). Observations of open-ocean deep convection in the northwestern Mediterranean Sea: Seasonal and interannual variability of mixing and deep water masses for the 2007-2013 Period. *Journal of Geophysical Research: Oceans*, *121*, 8139–8171. https://doi.org/10.1002/2016JC011857

Juza, M., Escudier, R., Vargas-Yez, M., Mourre, B., Heslop, E., Allen, J., & Tintor, J. (2019). Characterization of changes in western intermediate water properties enabled by an innovative geometry-based detection approach. *Journal of Marine Systems*, *191*, 1–12. https://doi.org/10.1016/j.jmarsys.2018.11.003

Juza, M., Mourre, B., Lellouche, J.-M., Tonani, M., & Tintoré, J. (2015). From basin to sub-basin scale assessment and intercomparison of numerical simulations in the Western Mediterranean Sea. *Journal of Marine Systems*, *149*, 36–49. https://doi.org/10.1016/j.jmarsys.2015.04.010

Juza, M., Mourre, B., Renault, L., Gómara, S., Sebastián, K., Lora, S., et al. (2016). SOCIB operational ocean forecasting system and multi-platform validation in the Western Mediterranean Sea. *Journal of Operational Oceanography*, *9:sup1*, s155–s166. https://doi.org/10.1080/1755876X.2015.1117764

Lana, A., Marmain, J., Fernández, V., & Tintoré, J. (2016). Wind influence on surface current variability in the Ibiza Channel from HF Radar. *Ocean Dynamics*, *66*, 483–497. https://doi.org/10.1007/s10236-016-0929-z

Levitus, S., Antonov, J. I., Boyer, T. P., Baranova, O. K., Garcia, H. E., Locarnini, R. A., et al. (2012). World ocean heat content and thermosteric sea level change (02000 m), 19552010. *Geophysical Research Letters*, *39*, L10603. https://doi.org/10.1029/2012GL051106

López-Jurado, J. L., & Díaz del Río, G. (1994). Dinámica asociada a las masas de agua en el canal de ibiza Ibiza en Noviembre de 1990 y Marzo de 1991. *Boletin del Instituto Espanol de Oceanografia*, *10*(1), 3–22.

López-Jurado, J. L., Marcos, M., & Monserrat, S. (2008). Hydrographic conditions affecting two fishing grounds of Mallorca Island (Western Mediterranean): During the IDEA Project (20032004). *Journal of Marine Systems*, *71*(34), 03–315. https://doi.org/10.1016/j.jmarsys.2007.03.007

MEDOC-Group (1970). Observation of formation of deep water in the Mediterranean Sea. *Nature*, *227*, 1037–1040. https://doi.org/10.1038/2271037a0

Marshall, J., & Schott, F. (1999). Open-ocean convection: Observations, theory, and models. *Reviews of Geophysics*, *37*(1), 1–64. https://doi.org/10.1029/98RG02739

Mason, E., & Pascual, A. (2013). Multiscale variability in the Balearic Sea: An altimetric perspective. *Journal of Geophysical Research: Oceans*, *118*, 3007–3025. https://doi.org/10.1002/jgrc.20234

McWilliams, J. C. (1985). Submesoscale, coherent vortices in the ocean. *Reviews of Geophysics*, *23*(2), 165–182. https://doi.org/10.1029/RG023i002p00165

Nurser, A. J. G., & Bacon, S. (2014). The Rossby radius in the Arctic Ocean. *Ocean Science*, *10*(6), 967–975. https://doi.org/10.5194/os-10-967-2014

Pascual, A., Buongiorno Nardelli, B., Larnicol, G., Emelianov, M., & Gomis, D. (2002). A case of an intense anticyclonic eddy in the Balearic Sea (western Mediterranean). *Journal of Geophysical Research*, *107*(C11), 3183. https://doi.org/10.1029/2001JC000913

Pascual, A., & Gomis, D. (2003). Use of surface data to estimate geostrophic transport. *Journal of Atmospheric and Oceanic Technology*, *20*(6), 912–926. https://doi.org/10.1175/1520-0426(2003)020<0912:UOSDTE>2.0.CO;2

Pascual, A., Ruiz, S., Olita, A., Troupin, C., Claret, M., Casas, B., et al. (2017). A multiplatform experiment to unravel meso- and submesoscale processes in an intense front (AlborEx). *Frontiers in Marine Science*, *4*, 39. https://doi.org/10.3389/fmars.2017.00039

Pascual, A., Vidal-Vijande, E., Ruiz, S., Somot, S., & Papadopoulos, V. (2014). Spatiotemporal variability of the surface circulation in the western mediterranean. In *The Mediterranean Sea* (Chap. 2, pp. 5–23). Washington, DC: American Geophysical Union. https://doi.org/10.1002/9781118847572.ch2

Pinot, J.-M., & Ganachaud, A. (1999). The role of winter intermediate waters in the spring-summer circulation of the Balearic Sea 1. Hydrography and inverse box modeling. *Journal of Geophysical Research*, *104*(C12), 29,843–29,864. https://doi.org/10.1029/1999JC900202

Pinot, J.-M., López-Jurado, J. L., & Riera, M. (2002). The CANALES experiment (1996-1998). Interannual, seasonal, and mesoscale variability of the circulation in the Balearic Channels. *Progress in Oceanography*, *55*(3-4), 335–370. https://doi.org/10.1016/S0079-6611(02)00139-8

Pinot, J.-M., Tintoré, J., & Gomis, D. (1995). Multivariate analysis of the surface circulation in the Balearic Sea. *Progress in Oceanography*, *36*(4), 345–376. https://doi.org/10.1016/0079-6611(96)00003-1

Rudnick, D. L., Zaba, K. D., Todd, R. E., & Davis, R. E. (2017). A climatology of the California Current System from a network of underwater gliders. *Progress in Oceanography*, *154*, 64–106. https://doi.org/10.1016/j.pocean.2017.03.002

Ruiz, S., Font, J., Emelianov, M., Isern-Fontanet, J., Millot, C., Salas, J., & Taupier-Letage, I. (2002). Deep structure of an open sea eddy in the Algerian Basin. *Journal of Marine Systems*, *33-34*, 179–195. https://doi.org/10.1016/S0924-7963(02)00058-1

Ruiz, S., Pascual, A., Garau, B., Faugère, Y., Alvarez, A., & Tintoré, J. (2009). Mesoscale dynamics of the Balearic Front, integrating glider, ship and satellite data. *Journal of Marine Systems*, *78*(Supplement), S3–S16. https://doi.org/10.1016/j.jmarsys.2009.01.007

Schaeffer, A., Roughan, M., Austin, T., Everett, J. D., Griffin, D., Hollings, B., et al. (2016). Mean hydrography on the continental shelf from 26 repeat glider deployments along southeastern australia. *Scientific Data*, *3*, 160070. https://doi.org/10.1038/sdata.2016.70

Schroeder, K., Chiggiato, J., Josey, S. A., Borghini, M., Aracri, S., & Sparnocchia, S. (2017). Rapid response to climate change in a marginal sea. *Scientific Reportsvolume*, *7*, 4065. https://doi.org/10.1038/s41598-017-04455-5

Testor, P., Bosse, A., Houpert, L., Margirier, F., Mortier, L., Legoff, H., & Conan, P. (2018). Multiscale observations of deep convection in the northwestern Mediterranean Sea During winter 20122013 using multiple platforms. *Journal of Geophysical Research: Oceans*, *123*, 1745–1776. https://doi.org/10.1002/2016JC012671

Testor, P., Send, U., Gascard, J.-C., Millot, C., Taupier-Letage, I., & Béranger, K. (2005). The mean circulation of the southwestern Mediterranean Sea: Algerian Gyres. *Journal of Geophysical Research*, *110*, C11017. https://doi.org/10.1029/2004JC002861

Tintoré, J., Vizoso, G., Casas, B., Heslop, E., Pascual, A., Orfila, A., et al. (2013). SOCIB: The Balearic Islands coastal ocean observing and forecasting system responding to science, technology and society needs. *Marine Technology Society Journal*, *47*(1), 101–117. https://doi.org/10.4031/MTSJ.47.1.10

Troupin, C., Beltran, J. P., Heslop, E., Torner, M., Garau, B., Allen, J., et al. (2015). A toolbox for glider data processing and management. *Methods in Oceanography*, *13-14*, 13–23. https://doi.org/10.1016/j.mio.2016.01.001